ELSEVIER

Radiation transport and density effects in non-equilibrium plasmas

Vladimir I. Fisher*, Dimitri V. Fisher, Yitzhak Maron

Faculty of Physics, Weizmann Institute of Science, Rehovot 76100, Israel

Abstract

We describe a model for self-consistent computations of ionic level populations and the radiation field in transient non-equilibrium plasmas. In this model, the plasma density effects are described using the effective-statistical-weights (ESW) formalism based on the statistics of the microscopic environment of individual ions. In comparison to earlier work, the ESW formalism is expanded to a self-consistent treatment of the radiative transfer. For non-Maxwellian plasmas, the atomic-kinetics and radiative transfer computations may be performed for an arbitrary distribution of the free electrons. A plasma is presented by a finite number of cells, each with uniform thermodynamic parameters. The radiation field in each cell is computed by accounting for the radiation of entire plasma and of external sources. To demonstrate the predictions of the ESW approach and their difference from those of the traditional approach we apply the model to high-density plasmas. Based on hydrodynamic simulations of a laser-matter interaction, we use the model to analyze spectral line shapes, where the effects caused by the spatial dependence of the plasma flow velocity are demonstrated. In single-cell simulations, for acceleration of the computations, the model utilizes recently derived formula for the cell volume−average and direction−average specific intensity of radiation.
© 2007 Elsevier B.V. All rights reserved.

1. Introduction

Determination of the radiation field and ionic level populations in plasmas is important for understanding the plasma dynamics and for interpretation of spectroscopic data. In the present paper, we describe a model for self-consistent computations of these quantities. The model is applicable to transient non-equilibrium non-Maxwellian plasmas. For a chemical mixture the description is detailed only for a single chemical element, while ions of the other elements are treated as *background ions* that have no quantum states. The background ions are characterized by the number density $n_b(\mathbf{r}, t)$ and a mean ion charge $Z_b(\mathbf{r}, t)$. They affect the Debye radius, the plasma coupling parameters, and the free−free radiation. The electron density $n_e(\mathbf{r}, t)$ is determined by the plasma neutrality condition.

2. Rate equations and the radiation field

In general, the plasma of interest is treated in terms of a 3D sequence of cells, each having uniform ion density $n_i(j, t)$ and temperature $T_i(j, t)$, where j is the cell number. For each cell the distribution of ions (atoms) over the energy levels is given by the non-LTE rate equations [1,2]

$$\frac{dN_q}{dt} = \sum_{q' \neq q} N_{q'} R_{q'q} - N_q \sum_{q' \neq q} R_{qq'},$$

where N_q is the number of ions in the q-th energy level and $R_{q,q'}$ is the rate of direct (single step) transition from the level q to the level q' due to all atomic-kinetics processes. $\sum_q N_q$ is the total number of ions in the cell, not including the background ions. Accounted for in the $R_{q,q'}$ matrix are: spontaneous radiative decay, autoionization, photoionization, electron impact ionization (including a removal of few electrons in one collision [3]), electron impact excitation, photoexcitation,

* Corresponding author. Fax: +972 8 934 2137.
  E-mail address: v.fisher@weizmann.ac.il (V.I. Fisher).

and the reverse processes. For ions a Maxwellian distribution is assumed. Transitions caused by thermal ion–ion collisions usually have small effect on the level populations [1,4,5] and are not included yet.

The local radiation field and, thus, the local distribution of photons $f_\nu(\mathbf{r}, t, h\nu)$ is computed self-consistently with the plasma composition and external radiation. The distribution of free electrons, $f_e(j, t, \varepsilon_e)$, is not self-consistent at present; however, for analysis of non-Maxwellian plasmas the electron impact transition rates may be computed for arbitrary $f_e(j, t, \varepsilon_e)$, where ε_e is the energy of free electron.

For each particular problem, the computations require Grotrian diagrams, oscillator strengths, autoionization probabilities, electron impact ionization cross-sections, electron impact excitation cross-sections, and photoionization cross-sections. The cross-section of any reverse process is determined by the principle of detailed balance [6]. Atomic-data, required for present work, are computed [7] using modern versions of the ATOM and MZ codes [8,9] and selected from Internet-accessible data bases [10].

The rates of the photoinduced processes depend on the local direction–averaged specific intensity of radiation. Since the entire cell is characterized by a single set of rates, the rates depend on the specific intensity space-averaged and direction–averaged over the cell, i.e. on:

$$\bar{I}_\nu(j,t) = \frac{1}{4\pi V_j(t)} \int\limits_{(V_j)} d\mathbf{r} \int\limits_{(4\pi)} d\mathbf{\Omega} I_\nu(\mathbf{r}, \mathbf{\Omega}, t). \tag{1}$$

Here, $V_j(t)$ is the cell volume and $I_\nu(\mathbf{r}, \mathbf{\Omega}, t)$ is the solution of the radiative-transfer equation [1,4]

$$\frac{\partial I_\nu(\ell,t)}{\partial \ell} = \epsilon_\nu(\ell,t) - \kappa'_\nu(\ell,t) I_\nu(\ell,t) \tag{2}$$

for a certain point $\mathbf{r}$ and direction $\mathbf{\Omega}$, ℓ is the coordinate along the line traversing the point $\mathbf{r}$ at the direction $\mathbf{\Omega}$, ϵ_ν is the emissivity, and κ'_ν is the opacity (corrected for the stimulated emission). Evidently, each of the lines may traverse many cells. External radiation sources are included in the boundary condition.

A correct description of the photoinduced transitions requires a computation of $\bar{I}_\nu(j,t)$, which includes low energy photons emitted due to transitions between close levels as well as higher energy photons emitted due to recombination to the ground levels or to deep vacancies. For this broad spectral range, we use non-uniform photon-energy grid, which resolves the shape of each spectral line. The typical number of the grid points (spectral groups) is 10^4–10^5.

In the computations of spectral line shapes the Doppler broadening, due to ion thermal motion and plasma turbulence, Stark-broadening, opacity broadening, and Doppler shifts are included. For the Stark-broadening computations we follow Baranger [2] or use the line shapes calculated based on Ref. [11].

Note that the fivefold integration (1), which has to be performed for each spectral group and time step, makes the computations time-consuming. However, for one important case, the integration can be avoided, as discussed in the next Section.

3. Radiation in a solitary cell

If a plasma is approximated by a single spherical or cylindrical cell and if the external radiation is negligible in comparison to the plasma radiation, the computations of $\bar{I}_\nu$ can be accelerated by orders of magnitude due to the tables available in Ref. [12], where it is shown that the fivefold integral (1), in the case of a solitary *spherical* cell, can be transformed to the simple expression:

$$\bar{I}_{\nu,s} = \frac{\epsilon_\nu}{\kappa'_\nu}(1 - e^{-\tau_R}) K_s(\tau_R), \tag{3}$$

with the tabulated function $K_s(\tau_R)$. Here, the subscript s denotes a sphere, $\tau_R \equiv \kappa'_\nu R$, and R is the sphere radius. Notice that $(\epsilon_\nu/\kappa'_\nu)(1 - e^{-\tau_R})$ is the radiation intensity in the sphere center, $I_\nu(0, \mathbf{\Omega})$. The function $K_s(\tau_R)$ increases from 0.75 to 1 for τ_R in the range $[10^{-3}, 10^4]$.

For a solitary *cylindrical* cell of a diameter D and a height H, the expression (1) can be transformed [12] to the expression:

$$\bar{I}_{\nu,c} = \frac{\epsilon_\nu}{\kappa'_\nu}(1 - e^{-\tau_R}) K_c(H/D, \tau_R), \tag{4}$$

where the subscripts c denote a cylinder, see Ref. [12] for details.

4. The plasma density effects

In the previous Section, we considered a plasma of relatively low density, therefore, for simplicity, the density effects were the traditional approach is described, for example, in Ref. [2]. In this approach, it is assumed that all ions of a given ionization stage are immersed in an identical local environment and, consequently, have an identical level scheme. Also assumed is that only two types of electron states are possible, namely, the unperturbed single-ion bound states and the free electron states. The traditional approach is widely used due to its simplicity; however, this simplicity causes some serious shortcomings, see the discussion in Refs. [13,14].

To correct for these shortcomings, the ESW approach has been developed, see Refs. [15,16] and references therein. This approach utilizes statistical data on the microscopic environment of individual ions and describes three types of electron states: bound, collectivized, and free. The collectivization of a bound electron is governed by the local arrangement of the perturbing ions and electrons around the parent ion, thus any state is collectivized only in a fraction of the ions, so that the collectivization is described statistically. In the present model, the ESW formalism is expanded for the self-consistent treatment of the radiative transfer.

To compare the traditional and ESW approaches we consider a thin disc ($H = 5$ μm, $D = 100$ μm) of aluminum plasma, see

Fig. 1, with an ion density $n_i = 6 \times 10^{21}$ cm^{-3} and a temperature $T_e = T_i$ that is 1 keV in central part of the disc ($r < 25$ μm) and 500 eV in the outer part (25 μm $< r <$ 50 μm). The radiation emitted along a diameter is simulated for a plasma in a collisional-radiative steady-state. A striking result is that the continuum edges are smoothed in the ESW approach, while the traditional approach predicts sharp edges. The smoothing is caused by the statistics of the local environment of the recombining ions. Another important difference is that the lines from levels with $n > 4$ are well resolved in the traditional approach, but are missing here as the effective-statistical-weights of these levels are much smaller than their nominal statistical weights. Lines from $n = 4$, Lyγ and Heγ, are well resolved in the both approaches; however, there is a substantial difference in the peak intensities, widths, and shapes predicted by the two approaches. For the resonance lines from low-lying levels ($n = 3$ and 2) at the density considered here, 0.10 of solid, the differences between the two approaches are rather small.

The differences in the radiation spectra computed in the two approaches are caused by the differences in local opacities and emissivities, which, in turn, are caused by the differences in the ionic level populations. For example, for the He-like and H-like ionization stages in the central part of the disc, the ESW approach yielded 0.6 and 14% of the total ion number, respectively, while the traditional approach gave 1.6 and 24% for these ionization stages.

Present comparison of the approaches is done for a steady-state plasma. In transient plasmas the ionization and recombination via collectivized states result in even stronger effect on the level populations [15] and thus on the line ratios.

5. Plasma flow effect on the spectral line shapes

Now we consider the interaction of a laser beam with a 20-μm thick Al foil in vacuum. The laser ($\lambda_L = 1.06$ μm) pulse variation with time is given by $q_L(t) = \widehat{q}_L \sin^2(\pi t_{ns}/2_{ns})$ with a FWHM = 1 ns and a peak intensity $\widehat{q}_L = 100$ TW/cm^2 within the focal spot of a radius $r_L = 0.5$ mm.
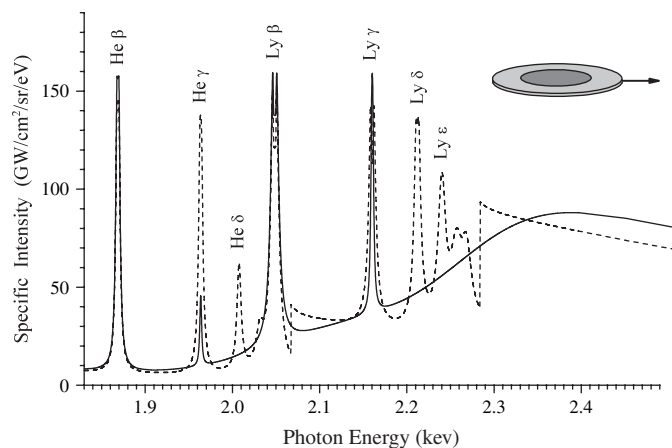
The laser beam direction is normal to the foil. Hydrodynamic simulations are performed [17] with MULTI-FS, a two-temperature Lagrangian 1D code with electron heat conduction and multi-group radiation transport [18,19].

The plasma density $n_i(j, t)$, flow velocity $u(j, t)$, and temperatures, determined in the hydrodynamic simulation, are used as an input for self-consistent computations of the ionic level populations and local radiation intensity $\overline{I}_\nu(j, t)$ in 150 cells. In the radiative-transfer computations we assume that the plasma jet is of the radius r_L and the hydrodynamic parameters are independent of the radial coordinate. The 1D approach to the problem is justified by the observation that during the plasma radiation burst, the thickness Δz of the main radiation source and its distance from the initial location of the foil are much smaller than r_L [20]. In the simulations, computed is the plasma radiation emitted towards a monochromator that views the focal spot center at 10° relative to the plasma jet symmetry axis.

In each of the plasma cells, the spectral shapes $p_{ul}(j, \nu)$ of the bound–bound emissivity and opacity are governed by the thermal motion of individual emitting ions (thermal Doppler effect) and Stark effect consistent with the temperatures and density in the cell. A spectral line $u \rightarrow l$, radiated by the entire plasma, is broader than $p_{ul}(j, \nu)$ due to the optical thickness in the observation direction and the spatial dependence of the plasma flow velocity, $u_{\mathbf{\Omega}}(j, t)$, in this direction. The spatial dependence $u_{\mathbf{\Omega}}(j, t)$ causes a sequence of Doppler shifts of the spectral line center, thus affecting both the widths and symmetry of the spectral lines along a given line of sight. An example of the asymmetry is shown in Fig. 2 for Lyα. For clarity the satellites to the Lyα were excluded in this simulation by excluding the autoionizing states from the list of acting levels.

The importance of the radiative-transfer along the jet for proper simulation of Lyα shape in laser-produced plasmas was emphasized in Ref. [21]. However, since that study was focused on the relative intensity of the Lyα components, the plasma flow effect was minimized by observing the plasma normally to its symmetry axis.

Fig. 1. The radiation along the diameter of a cylindrical disc of a dense aluminum plasma. Dashed: the traditional approach; solid: the ESW approach.
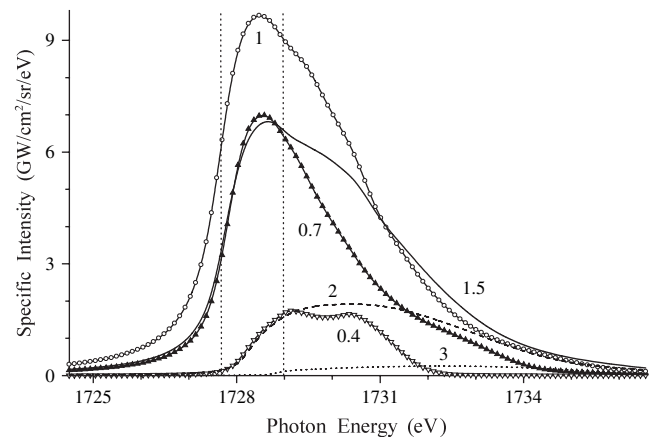
Fig. 2. The evolution of the Lyα shape. The numbers near the curves give the times in nanosecond. The two vertical dotted lines mark the centers of the Lyα components in a motionless plasma.

6. Summary

We have presented a brief description of our atomic-kinetics and radiative-transfer model. The main features of this model are (a) the self-consistency of the local level populations and the local radiation field, (b) the plasma density effects treatment that is based on the statistics of the microscopic environment of individual ions, and (c) the applicability to non-Maxwellian plasmas. For solitary plasma cells we indicated the existence of expressions (3) and (4) that can be used for rapid rigorous computations of photoinduced transition rates.

We have presented, for the first time, dense plasma radiation spectra computed using the effective-statistical-weights approach with an account of the radiative transfer. Large differences between the more realistic radiation spectrum, predicted by the ESW approach, and that predicted by the traditional approach are shown. Finally, we demonstrated the combined effects of the plasma flow velocity gradient and radiative transfer on the spectral line broadening and shape asymmetry in a laser-produced plasma.

References

[1] D. Mihalas, B. Weibel-Mihalas, Foundations of Radiation Hydrodynamics, Oxford University Press, Oxford, 1984.
[2] H.R. Griem, Principles of Plasma Spectroscopy, Cambridge University Press, Cambridge, 1997.
[3] V. Fisher, Yu. Ralchenko, A. Goldgirsh, D. Fisher, Y. Maron, J. Phys. B 28 (1995) 3027.
[4] Ya.B. Zel'dovich, Yu.P. Raizer, Physics of Shock Waves and High-Temperature Hydrodynamics Phenomena, Academic Press, New York, 1967.
[5] This is due to the low (in the sense of the Massey adiabatic criterion [4,22]) ionic thermal velocity that results in small ion−ion inelastic cross-sections (except for transitions between close levels) and in low transition rates [1,4,22]. For close levels, the ionic impact effect may be illustrated by the atomic-kinetics computations performed with the account of ion−ion collisions [23]. These computations showed the differences of a few-percent in the population ratio of the $2p_{1/2}$ and $2p_{3/2}$ levels of H-like aluminum ($\Delta E = 1.3$ eV) for T_i between $T_e/4$ and $4T_e$, where $T_e = 1$ and 4 keV in aluminum plasma of $n_e = 10^{19}$ and 10^{20} cm^{-3}. Another type of the adiabatic ion−ion transitions, known as the resonant charge transfer, has relatively large cross-sections in *binary* collisions; however, *in plasmas* the probability of resonant charge transfer decreases strongly with density due to the electric field of neighboring ions [24].
[6] J. Oxenius, Kinetic Theory of Particles and Photons, Springer-Verlag, Berlin, 1986 (chapter 1).
[7] This work is performed by Yu.V. Ralchenko, V.A. Bernshtam, A. Starobinets, A. Goldgirsh, L. Weingarten, private communication.
[8] I.I. Sobelman, L.A. Vainshtein, E.A. Yukov, Excitation of Atoms and Broadening of Spectral Lines, Springer-Verlag, Berlin, 1995.
[9] V.P. Shevelko, L.A. Vainshtein, Atomic Physics for Hot Plasmas, IOP Publishing, Bristol, 1993.
[10] Yu. Ralchenko, JQSRT 99 (2006) 499.
[11] E. Stambulchik, Y. Maron, JQSRT 99 (2006) 730.
[12] V.I. Fisher, I.R. Almiev, Y. Maron, Preprint WIS/26/05-Sept-DPP, Weizmann Institute of Science (2005).
[13] V.E. Fortov, I.T. Yakubov, Physics of Nonideal Plasma, Hemisphere Publication Corporation, New York, 1990.
[14] M.J. Seaton (Ed.), The Opacity Project, vol. 1, Institute of Physics Publishing, Bristol, 1995.
[15] D.V. Fisher, Y. Maron, JQSRT 81 (2003) 147.
[16] D.V. Fisher, Y. Maron, Eur. Phys. J. D 18 (2002) 93.
[17] The simulations by the MULTI-FS code are performed by Teodor Schlegel.
[18] K. Eidmann, J. Meyer-ter-Vehn, T. Schlegel, Phys. Rev. E 62 (2000) 1202.
[19] Recently, two advancements were made in the code. First, the plasma opacity and mean ion charge are tabulated as functions of density and temperature in the CRE approach, using simplified atomic database. Second, in the high-density limit, the transition to the Thomas−Fermi model is provided.
[20] V.I. Fisher, D.V. Fisher, Y. Maron, T. Schlegel, D.H.H. Hoffman, High Energy Density Physics with Intense Ion and Laser Beams: GSI report; p. 53; 2005.
[21] O. Renner, F.M. Kerr, E. Wolfrum, J. Hawreliak, D. Chambers, S.J. Rose, J.S. Wark, H.A. Scott, P. Patel, PRL 96 (2006) 185002.
[22] Earl W. McDaniel, J.B.A. Mitchell, M.E. Rudd, Atomic collisions, Heavy Particle Projectiles, John Wiley & Sons, New York, 1993, p. 136 (p. 378).
[23] J.M.A. Ashbourn, Phys. Rev. E 59 (1999) 6198.
[24] D.V. Fisher, J. Phys. B 36 (2003) 4107.